Performance of a 500-kjoule MHD Wind Tunnel

W. R. GRABOWSKY,* D. A. DURRAN,† AND H. MIRELS‡
The Aerospace Corporation, El Segundo, Calif.

The operation of a pulsed MHD accelerator is described for a MHD wind-tunnel application. The accelerator is designed to provide a 50% velocity increase (from 15.5 kft/sec to 24 kft/sec), at constant enthalpy, of a gas at approximately atmospheric pressure. The accelerator gas source is a hot shot that heats potassium seeded nitrogen to 9000°K and 1400 atm. The gas is expanded into a segmented electrode (94 pair) MHD accelerator channel. After tunnel startup, a 3-msec constant power pulse is switched on the electrodes so that current flow is approximately perpendicular to a quasi-steady 4-wb/m² magnetic field. The power-on to power-off velocity ratio ($\equiv u_n/u_f$) at the accelerator exit is determined from changes in the stagnation pressure and open circuit induced potential. The corresponding enthalpy ratio ($\equiv h_n/h_f$) is determined from the static pressure change and u_n/u_f. Results 0.5 msec after switch-on indicate $u_n/u_f \approx 1.5$ ($u_n \approx 24$ kft/sec) and $h_n/h_f \approx 1.0$. As a result of constant volumetric power addition and a decaying mass flow, u_n/u_f and h_n/h_f increase to 1.7 and 1.2, respectively, just prior to channel power switch-off. Although these results are essentially the design values, the detailed performance of the accelerator appears to be significantly influenced by spatial nonuniformities in the flow.

Nomenclature

$A,\bar{A}$ = area, $\bar{A} = A/A_1$
$B,\bar{B}$ = magnetic field strength (z direction), $\bar{B} = B/B_1$
b = cross-channel dimension $[=(A)^{1/2}]$
C = capacitance
d = diameter
$E,\bar{E}$ = electric field intensity (y direction), $\bar{E} = E/u_1B_1$
E_x = electric field intensity (x direction)
$h,\bar{h}$ = enthalpy, $\bar{h} = h/u_1^2$
i = electrode number
$J,\bar{J}$ = current density (y direction), $\bar{J} = J/\sigma_1 u_1 B_1$
J_x = current density (x direction)
I = current
I_B = magnetic field capacitor bank current
I_c = magnetic field coil current
I_x = magnetic field crowbar current
L = inductance, accelerator length
L_1 = interaction length ($\equiv \rho_1 u_1/\sigma_1 B_1^2$)
$\dot{m}$ = mass flow
N = total number of electrode pairs fed by one pulse forming network
n = velocity exponent
$\bar{P}$ = constant, ratio of inlet to dynamic pressure, $(P_1/\rho_1 u_1^2)$
$p,\bar{p}$ = pressure, $\bar{p} = P/\rho_1 u_1^2$
P_t = channel stagnation pressure
R = gas constant
r = upper electrode resistance
S = entropy
T = temperature
t = time
U = induced potential ($\equiv |\mathbf{u} \times \mathbf{B}| b$)
$u,\bar{u}$ = velocity, $\bar{u} = u/u_1$
V_B = magnetic field capacitor bank voltage
V_L = electrode feed system lower bus potential
V_l = lower electrode potential
V_U = electrode feed system upper bus potential
V_u = upper electrode potential
$x,\bar{x}$ = axial coordinate, $\bar{x} = x/L_1$
Z_L = pulse forming network characteristic line impedance
α = constant in area equation $= \frac{1}{2}[(\bar{E}_1 - 1)/\bar{E}_1\bar{P} - 1]$
β = Hall parameter
γ = ratio of specific heats
ϕ = constant of proportionality $= \bar{E}_1(\bar{E}_1 - 1)$
η = efficiency
ρ = lower electrode resistance, density
$\sigma,\bar{\sigma}$ = electrical conductivity, $\bar{\sigma} = \sigma/\sigma_1$
τ = hot-shot jitter time, Fig. 4

Subscripts

$(\ )_1$ = accelerator entrance quantity
$(\ )_e$ = accelerator exit quantity

Presented as Paper 68-370 at the AIAA 3rd Aerodynamic Testing Conference, San Francisco, Calif., April 8–10, 1968; submitted April 8, 1968; revision received December 27, 1968. This paper was prepared under U.S. Air Force Contract F04695-67-C-0158.

* Senior Staff Scientist, Laboratories Division. Member AIAA.

† Member Technical Staff, Aerodynamic and Propulsion Research Laboratory. Member AIAA.

‡ Head, Aero and Heat Transfer Laboratories Division. Associate Fellow AIAA.

I. Introduction

THE use of a Faraday-type MHD accelerator to augment the test capabilities of aerodynamic wind tunnels is being investigated by a number of organizations. Theoretical studies describing potential improvements in wind-tunnel performance are discussed in Refs. 1 and 2.

The experimental performance of MHD accelerators, under conditions encountered in MHD wind tunnels (i.e., pressure $\gtrsim 1$ atm), remains a major uncertainty and is under investigation at several laboratories, including Arnold Engineering Development Center (AEDC), General Electric Company (GE), and the Aerospace Corporation. The AEDC effort includes studies in 4 Mw[3] and 20 Mw[4] continuous flow pilot facilities that use electric arcs as a source. The gas is seeded with potassium to enhance its electrical conductivity. Increases in velocity of a factor of ~ 2 (exit velocity ≈ 10 kft/sec) have been reported for the 4-Mw facility. Another AEDC effort, as well as the one at GE,[5] employs a shock tunnel as the source. These facilities have test times of the order of 1 msec.

The Aerospace MHD accelerator test facility is of the pulsed type and employs a hot shot as a source of high-temperature seeded gas. The test time is 3 msec. The total energy used to power the hot shot, accelerator electrodes, and magnetic field is ≈ 500 kjoule. An accelerator channel is being investigated that is designed to accelerate nitrogen from $u_1 = 15.5$ kft/sec, $p_1 = 5.5$ atm, and $T_1 = 4000°$K to $u_e = 24$ kft/sec, $p_e = 1.5$ atm, and $T_e = 4000°$K. This accelerator channel is 2.5 ft long and has 94 segmented electrode pairs.

II. Analytic Studies and Design

The design of the accelerator is based on a closed-form solution for a one-dimensional MHD accelerator flow that assumes a constant enthalpy $\bar{h} = 1$, a specified area variation $\bar{A} = (1 + \alpha\phi\bar{x})^2$, and an energy addition per unit length proportional to a power of the velocity, $\bar{J}\bar{E}\bar{A} = \phi\bar{u}^n$. The constant enthalpy assumption prevents degradation of altitude simulation and minimizes the dissociation of the working fluid for high-pressure flows that would result from higher fluid temperatures. The assumed area variation results in a right, truncated, square-pyramid, channel geometry that is easily constructed and is consistent with shock-free supersonic flow. The last assumption insures that the power addition per unit length can be reasonably distributed over the accelerator length.

From Ref. 6, the governing equations with the stated assumptions are (in nondimensional form):

$$\bar{\rho}\bar{u}\bar{A} = 1 \tag{1}$$

$$\bar{\rho}\bar{u}\, d\bar{u}/d\bar{x} = -d\bar{p}/d\bar{x} + \bar{J}\bar{B} \tag{2}$$

$$u\, d\bar{p}/d\bar{x} = -\bar{J}^2/\bar{\sigma} \tag{3}$$

$$\bar{J} = \bar{\sigma}(\bar{E} - \bar{u}\bar{B}) \tag{4}$$

$$\bar{p} = \bar{\rho}/\bar{P} \text{ (perfect gas)} \tag{5}$$

$$\bar{\sigma} = \bar{\sigma}(\bar{\rho},\bar{h}) \tag{6}$$

Equations (2–4) can be combined with $\bar{J}\bar{E}\bar{A} = \phi\bar{u}^n$, and the channel velocity can be found, viz.,

$$\bar{x} = (\bar{u}^{2-n} - 1)/\phi(2 - n) \quad (n \neq 2) \tag{7}$$

and

$$\bar{x} = \ln\bar{u}/\phi \quad (n = 2)$$

The density follows from Eq. (1) and from the assumed area distribution

$$\bar{\rho} = 1/\bar{u}\bar{A} \tag{8}$$

Since Eq. (5) has not been utilized in obtaining Eq. (7) or (8), these equations are valid for real gases. In addition, since $\bar{h}$ is constant and $\bar{\rho} = \bar{\rho}(\bar{x})$ is known, $\bar{p}(\bar{x})$ and $\bar{\sigma}(\bar{x})$ can be easily determined for real equilibrium gases, and $\bar{J}(\bar{x})$ can be evaluated from Eq. (3). For the accelerator design in question, however, the dissociated fraction in nitrogen is small ($\lesssim$2%). Consequently, Eq. (5) is applicable, and a closed form can be obtained for $\bar{J}$; i.e.,

$$\bar{J} = \left[\bar{\sigma}\bar{P}\phi\left(\frac{\bar{u}^{n-2} + 2\alpha/(\bar{A})^{1/2}}{\bar{A}}\right)\right]^{1/2} \tag{9}$$

With $\bar{J}$ known, $\bar{E}$ and $\bar{B}$ are easily determined, viz.,

$$\bar{E} = \phi\bar{u}^n/\bar{J}\bar{A} \tag{10}$$

and

$$\bar{B} = (\bar{E} - \bar{J}/\bar{\sigma})/\bar{u}. \tag{11}$$

Since α and ϕ are functions of $\bar{E}_1$ and $\bar{P}$, Eqs. (7) through (11) define the solution with $\bar{E}_1$, $\bar{P}$, and n as free parameters.

With this solution, the actual accelerator can be designed once the test-section conditions and the physical constraints on certain parameters of the facility are specified. The desired ultimate test condition that results from an expanding (frozen) accelerator flow was a velocity of 36 kft/sec at a simulated altitude of 250 kft, i.e., lunar re-entry conditions. Various lower-energy test points are obtainable and depend on the accelerator length.

Since this test condition was rather ambitious, the best possible source was required. A source stagnation condition in nitrogen of $T \approx 9000°$K and $p = 1400$ atm was selected as approximating the upper limit obtainable in the hot shots[7] or the reflected region of a shock tunnel.[8] For nitrogen (or air) seeded with ~1% potassium, the decay in σ with temperature is rather severe for $T \approx 4000°$K.[9,10] Thus, the source conditions were expanded to $T_1 \approx 4000°$K ($A_1/A^* \approx 20$), which established the inlet conditions for the accelerator. With the entrance enthalpy determined, the accelerator exit enthalpy was known ($h_e = 1100$ cal/g), and the remainder of the exit conditions were determined by "backing up" the point specified by the test altitude to the accelerator exit enthalpy. This procedure resulted in $p_e \approx 0.5$ atm and $u_e \approx 34$ kft/sec.

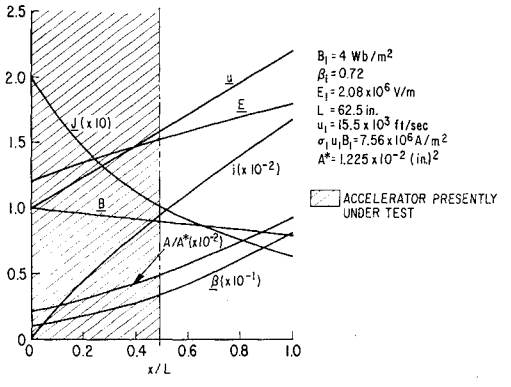

Fig. 1 MHD accelerator design.

With the accelerator entrance and exit conditions known, the accelerator design was accomplished by the described closed-form solution. The known inlet conditions determined $\bar{P}$, which was used with various values of $\bar{E}_1$ and n to obtain a $\bar{\sigma} = 1$ accelerator design that resulted in the desired exit conditions, that had reasonable distribution in $\bar{B}(x)$, $\bar{E}(x)$, etc., and that was consistent with certain physical constraints. The imposed constraints were: 1) a maximum magnetic field strength of 4 wb/m^2, 2) negligible ion-slip effects ($\beta_e \lesssim 10$), 3) a minimum accelerator length, 4) a total facility energy of $\lesssim$500 kjoule, and 5) a reasonable boundary-layer thickness compared with the channel width.

The final design values of some of the electrodynamic and gas-dynamic parameters within constraints 1, 2, and 3 are shown in Fig. 1. The design values of $\bar{E}_1$ and n were 1.2 and 1.0, respectively. Parameters of interest not shown in Fig. 1 are the flow Mach number and entropy. At the accelerator entrance $M \approx 4$ and $S/R = 31.8$, and at the exit $M \approx 9$ and $S/R = 34.1$. Later optimization studies[11] produced results similar to those obtained elsewhere[12] and showed that the above accelerator design was of minimum length to within a few percent.

Constraints on facility energy and boundary-layer thickness were satisfied by the selection of the accelerator geometry and the period of facility operation (test time). In particular, the facility energy is determined by the throat size, the mass-flow decay rate associated with the fixed volume of the hot-shot source, and the test time, whereas the ratio of boundary-layer thickness to channel width is affected only by the throat size for a given channel length. A d* = 0.125 in., mass-flow decay rate $[1/\dot{m}(t = 0)]d\dot{m}/dt = 10\%$/msec, and a test time of 3 msec were eventually selected as the design values. This resulted in a hot-shot volume of 86 cm^3, a total facility energy (efficiency = 1) of 250 kjoule (hot shot ~45 kjoule, $E \sim 40$ kjoule, $B \sim 165$ kjoule), and a boundary-layer thickness (using Refs. 13 and 14) of ~0.17 in. at the channel exit ($x/L = 1$). Although this boundary-layer thickness is somewhat large, it was considered acceptable in order to maintain the total energy required as small as possible.

The final channel geometry is shown in Fig. 1. Also indicated is the extent of the present experimental effort ($x_e = 2.5$ ft, 94 electrodes). The accelerator exit conditions at this point would expand into a test point slightly in excess of satellite re-entry conditions, i.e., $u \approx 26$ kft/sec at an altitude of ≈230 kft.

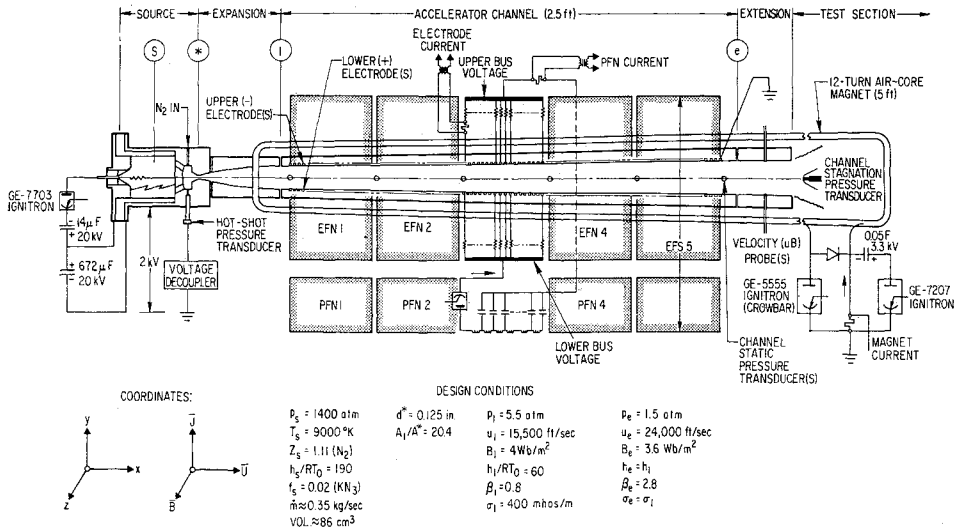

Fig. 2 MHD accelerator schematic.

III. Description of the Facility

Shown in Fig. 2 are the various components of the facility, which are all powered with capacitor banks. The timing sequence used to phase the operation of these components properly during facility operation is started with the initial rise of magnetic field. The air-core-magnet circuit parameters are so chosen that magnetic field variation with time is small during the 3-msec tunnel operating time. Approximately 2 msec after magnetic field start-up, the hot shot is fired. The hot-shot construction and circuit parameters result in essentially impulsive pressurization and heating of the gas. After a 1-msec delay, steady flow is established in the accelerator, and a 3-msec power pulse is applied to the accelerator electrodes.

Magnetic Field

The magnetic field coil and circuitry (Fig. 2) are detailed in Fig. 3. The 12-turn, 5-ft-long coil (designed for the full accelerator) produces the design B shown in Fig. 1. This axial variation was obtained by shimming the conductors with gauss meter readout while the magnet coil was carrying a small d.c. current (100 amp). During the shimming operation, departures from B in both perpendicular field components were less than 3% of B anywhere in the accelerator channel volume. After shimming, conductor position was maintained by potting with epoxy.

The magnetic field coil is powered by a 0.05-farads capacitor bank that delivers 42 ka to the coil when charged to 3.3 kv. This current produces the 4 wb/m² required at the accelerator entrance. Ignitrons are used for the switch (GE 7207) and crowbar (GE 5555); the use of the crowbar prevents the circuit from ringing, thereby increasing capacitor bank life and eliminating "magnet pumping." The crowbar ignitron is the most critical component in the circuit since manufacturers' specifications are exceeded by a factor of ~2. The diode array (diode D, Fig. 3) is used in the main capacitor bank circuit to block additional capacitor currents to the crowbar circuit; these currents result from small but finite resistance and inductance in the capacitor bank circuit. This effect can be seen in Fig. 3. Note that the magnet current I_B is the same in both cases, whereas the crowbar current is greater without the diode.

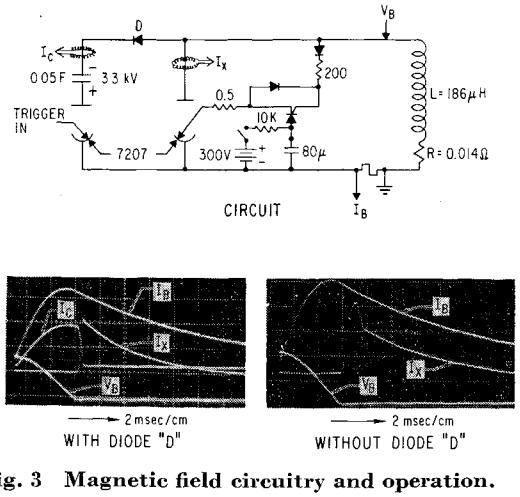

Fig. 3 Magnetic field circuitry and operation.

Hot Shot

Since the capacitively driven hot shot (Fig. 2) developed for this application has been described in detail in Ref. 15, only a brief description is given here. Because of the high-energy density of the source gas and the timing requirement on the hot-shot firing (i.e., fired relative to B), rapid heating and immediate use of the hot gas are essential. This is accomplished by maintaining a low inductance in the hot-shot circuit ($\lesssim$0.15 μh). The capacitor bank used to power the hot shot is rated at 130 kjoule at 20 kv and is sufficient to heat the initial 500-psig charge of nitrogen to the desired stagnation conditions even if the heating process is only 33% efficient. In practice, the electrical efficiency is essentially 100%, whereas the total heating efficiency is ≈50%.[15] Typical voltage and current traces and the resulting power and energy calculations are shown in Fig. 4. Gas heating has occurred in ~30 μsec, and the jitter time τ is ~20 μsec (typically $\tau = 25 \pm 10$ μsec). These characteristic times are compatible with the timing sequence.

The internal construction of the hot shot is shown schematically in Fig. 2. Virtually all surfaces of the hot-shot internal volume are either boron nitride or Mallory Elkonite 40W3. This construction results in an estimated contamination of ~6% (from weighings). An auxiliary capacitor is used to trigger the main capacitor bank; this capacitor generates and injects a plasma into a small gap "standing off" the main bank voltage. The discharge is initiated along a fine aluminum wire that is suspended from the center of the cathode and reaches to within 0.25 in. of the trigger plasma source in the center of the anode. To obtain an adequate conductivity level in the accelerator, it was necessary to seed the nitrogen source gas with potassium. Considerable effort was required to develop the seeding technique.[15] Successful seeding is obtained by sprinkling finely ground potassium azide (KN_3) on the chamber wall. Typically, $p = 1450 \pm 150$ atm and $T = 9200 \pm 300$°K are obtainable in the hot-shot

Table 1 Characteristic values for the first and fifth EFS

	EFS 1	EFS 5
Efficiency	0.33	0.31
Electrode pairs fed	20	18
Impedance, Ω	0.377	0.619
Charge voltage, v	1870	3350
Total current, amp	2475	2710
Energy, kjoule	6.95	14.31

chamber. The mass flow decay rate is approximately the design value.[15]

Accelerator and Electrode Feed System

The accelerator and the electrode feed system must successfully maintain $J_x = 0$ in a medium where the electrical conductivity is nonisotropic. To accomplish this, an axial component of electrical field E_x given by Ohms law must be imposed on the working fluid; i.e., $-J_x = \sigma E_x - \beta J = 0$ or $E_x = \pi/\sigma J$. Since the interaction length of an accelerator is defined

$$L_1 \equiv \rho_1 u_1/\sigma_1 B_1^2 = (u_1/\sigma_1 B_1)(1/B_1/\rho_1) = (u_1/\sigma_1 B_1)(1/\beta_1)$$

for reasonable lengths, a finite β_1 is required, confirming that $E_x \neq 0$, and the accelerator must be constructed so as to permit an E_x (electrode segmentation). The electrode feed system must apply the proper axial potential such that $J_x \approx 0$ and a transverse potential such that the proper current distribution is obtained.

The segmented-electrode MHD accelerator channel undergoing study is ~2.5 ft long, 0.5 in. square at the entrance, 0.78 in. square at the exit, contains 94 pairs of copper electrodes, and all insulating surfaces are boron nitride. The electrode segmentation spacing is equal to one-half the cross channel dimension at the beginning of each 6-in. (approximately) section, and this spacing is held constant for the remainder of the section. The electrodes are staggered so that the downstream edge of the anode is at the same axial location as the upstream edge of the corresponding cathode. The axial dimension of the electrodes is 0.074 in.

In most accelerator experiments, the axial electric field is obtained by the use of isolated electrode power supplies[3,5] or a slant electrode geometry.[16] In these experiments an electrode feed system (EFS), which is composed of an electrode feed network (EFN) and pulse forming network (PFN), applies the proper axial and cross channel potential to ~20 channel electrodes.[17]

The EFN is shown schematically in Fig. 5, which is also a potential vs axial distance plot for the channel. The EFN consists of upper and lower electrode resistors r_i and ρ_i each connected to a common bus. The value of the resistance is calculated from the local gasdynamic and thermodynamic conditions using design values or experimental results. When power is applied to the buses, the flow of the electrode current establishes the proper channel axial $V_{(i+1)} - V_i$ and cross channel $V_i - V_{u_i}$ potential, and $(J_x/J)^2$ will be small compared to unity. While the resistors r_i and ρ_i are a source of inefficiency, they do provide local current regulation that aids in maintaining a constant electrode current even in the presence of a fluctuating conductivity or velocity.[18]

A ten-section PFN is used as a power supply and is connected to the EFN by means of a standard ignitron (GE 7703). The PFN, switched on to the EFN bus after tunnel startup, produces a flat current pulse over the "test time," and shuts off after the energy stored in the PFN is delivered to the load. In addition, nondissipative total current regulation is provided during PFN discharge by the characteristic line impedance Z_L (equal to the input resistance to the EFN).

The EFS is thus formed by the marriage of the EFN and PFN. From Fig. 5, it is easily seen that the efficiency

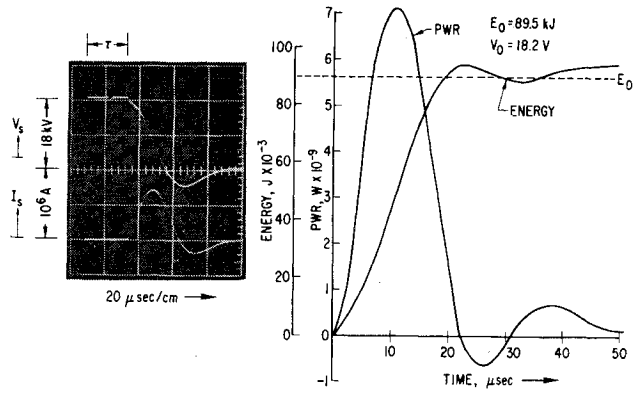

Fig. 4 Hot-shot electric characteristics.

$[\approx (V_i - V_{u_i})/(V_L - V_U)$ for $i = N/2, J_x = 0]$ decreases as N (electrode pairs/EFS) increases, and, consequently, feeding all 94 electrode pairs in the channel with one EFS is impractical. Therefore, five independent EFS's are utilized for the 94 electrode pairs (Fig. 2). The characteristic values for the first and fifth EFS are representative of the other three EFS's and are given in Table 1.

The efficiency (see Table 1) is greater for the EFS than for isolated electrodes powered by individual capacitors. It results from the inherent timewise current decay of a capacitor as compared to the current pulse from the EFS. If the channel is considered to have constant (timewise) resistance $= 2/b\sigma$ and induced potential uBb, the ratio of capacitor-voltage at any time t to initial voltage is $V(t)/V_0 = [I(t)/I_0] + (u_0 B_0/E_0)[1 - I(t)/I_0]$ where $(\ )_0$ is the quantity at $t = 0$. This can be related to a stored energy utilization efficiency η as

$$\eta = 1 - \left(\frac{V(t)^2}{V_0}\right) = 1 - \left[\frac{I(t)}{I_0} + \frac{u_0 B_0}{E_0}\left(1 - \frac{I(t)}{I_0}\right)\right]^2$$

Even for large current decays and independent of the actual discharge time, the efficiency is quite low, i.e., for $I(t)/I_0 = 0.5$ and $E_0/u_0 B_0 = 1.2$, $\eta = 0.16$, which is approximately a factor of 2 below the EFS η's utilized in this study.

IV. Instrumentation

A pulsed MHD accelerator poses complex instrumentation problems.[19] These are primarily associated with the large time-varying electric and magnetic fields generated during the experiment and with the axial channel potential. Such conditions require instrumentation that operates on the order of 10^3 v above ground (instrumentation reference voltage) and within a 4w/m² field.

The magnetic field measurement is obtained from a low-inductance current shunt. Since the magnetic field distribution for the coil was determined from d.c. measurements, a total current measurement gives the magnetic field everywhere throughout the channel.

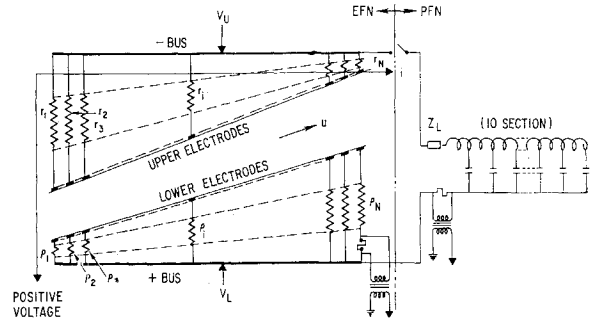

Fig. 5 Electrode feed system.

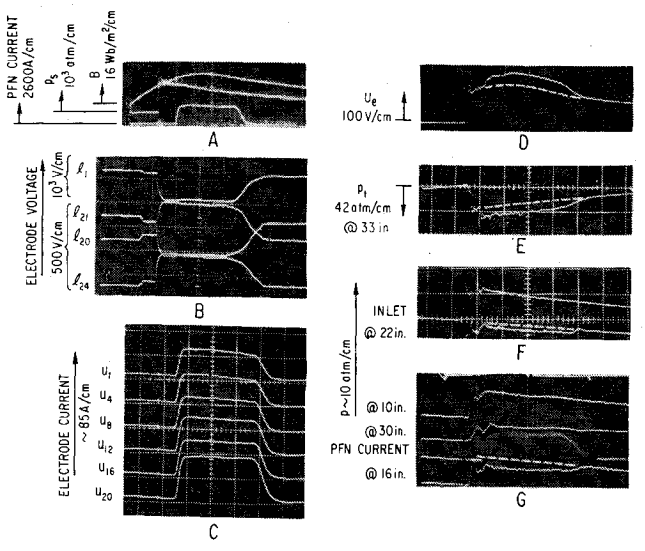

Fig. 6 MHD accelerator instrumentation 3 PSN's operating (all traces, 1 msec/cm).

The hot-shot pressure measurements are obtained by means of two different voltage decoupling schemes. The major difficulty encountered is that the axial potential along the accelerator ($\approx V_{l_1}$) raises the hot-shot potential to 2 kv above ground. One high-voltage decoupler[20] consists of a 19-MHz signal modulated by the hot-shot pressure transducer. This signal is fed through a high-frequency, high-voltage isolation transformer and then demodulated at near ground potential. The other decoupler[21] utilizes a photon-coupled isolator (Hewlett-Packard 4301). The current through the pressure transducer, at hot-shot potential, also flows through the GaAs diode of the isolator that emits infared radiation proportional to the current. This radiation is received at near ground potential by the isolator photodiode whose amplified output is displayed on an oscilloscope.

EFN bus voltage measurements are made with standard Tektronix P-6019 probes (input impedance of 100 MΩ). Typically, the downstream upper electrode (cathode) is grounded, and all bus voltages are measured with reference to this electrode. A 10-kΩ resistor (Fig. 2) is located between adjoining cathodes of adjacent EFS's to eliminate noise induced by magnetic field buildup prior to hot-shot firing.

Representative electrode currents are measured with low-inductance shunts that are transformer-coupled to the oscilloscope to eliminate the grounding problem. Both upper and lower electrode currents are measured. The channel potential distribution can be obtained by use of the bus voltage measurements and calculation of the voltage drop from the measured current through the known EFN resistors. In addition, these current measurements allow calculation of the axial and accelerating current densities required for accelerator performance calculations.

Channel static pressures are measured by means of the strain gauge pressure transducer described in Ref. 22. These transducers decouple the axial potential from the sensor by insulator surfaces that electrically isolate the strain gauges from the flow. Static pressure measurements are made at the entrance and the exit of the channel and between adjacent EFS's.

Channel stagnation pressure measurements are obtained from a transducer whose internal construction is similar to that of the static pressure gauge. Externally, the total pressure force is measured on the $\frac{1}{8}$-in.-diam, flat, copper face. The stagnation pressure measurement requires a small correction (~9%) for the pressure distribution over the flat-faced cylinder.[23] As a result of the high heat-transfer rates to the gauge face (~10 kw/cm²), the flat, copper face needs to be replaced after each run. Since $M > 3$, the stagnation pressure is $\approx \rho u^2$, and the change in the stagnation pressure during E application gives a direct measure of the velocity increase.

Additional velocity information can be obtained from the potential U induced on unpowered electrodes; i.e., for "slug" flow, $U = uBb$ for $J = 0$. Early work with the described hot-shot source[18] instrumented to measure U showed the velocity calculated from a U/Bb measurement to be low by a factor of 1.1 to 2 as compared to the u obtained from a one-dimensional expansion. (Typically values of $\lesssim 1.3$ came from electrodes protruding into the flow whereas values of ~2 came from flush mounted electrodes.) However, the measured static and stagnation pressures agreed with those calculated from a one-dimensional expansion. Furthermore, the decay in U/Bb with time was consistent with the expected hot-shot source-gas temperature decay (and corresponding decay in u) due to radiation loss and gas efflux. From these results, it was concluded that the one-dimensional (centerline) velocity u was $\propto U/B$. The measurement of U is obtained using common mode rejection and P-6012 voltage probes. This voltage is taken from flush-mounted electrodes $\sim 2b_e$ downstream of the last powered electrode.

All flow diagnostics were made within the magnetic field (per Fig. 2) and any affects resulting from the flow exiting the magnetic field have not been measured.

V. Results

Typical results obtained with this instrumentation are shown in Fig. 6. All traces are triggered simultaneously. The timing sequence is displayed in Fig. 6a, which shows the phasing of the magnetic field, the hot-shot pressure, and the accelerator current. There is an instantaneous rise (Fig. 6a) of the hot-shot gas pressure ~1.8 msec after magnetic field startup. The slow hot-shot pressure decay is characteristic of the hot-gas efflux from a fixed volume of source gas.[15] A flat 3-msec current pulse, which defines the "test period," is applied to the accelerator electrodes 1 msec after hot-shot pressurization and is phased with the magnetic field so that the minimum time variation in the magnetic field occurs during the test period. Figure 6a shows the PFN 1 current. All PFN's are fired simultaneously.

Figures 6b and 6c show electrode voltages and currents; both the voltage and the current are constant over the test period. Although the current pulses are similar to the PFN current in Fig. 6a, the amplitude varies slightly for different

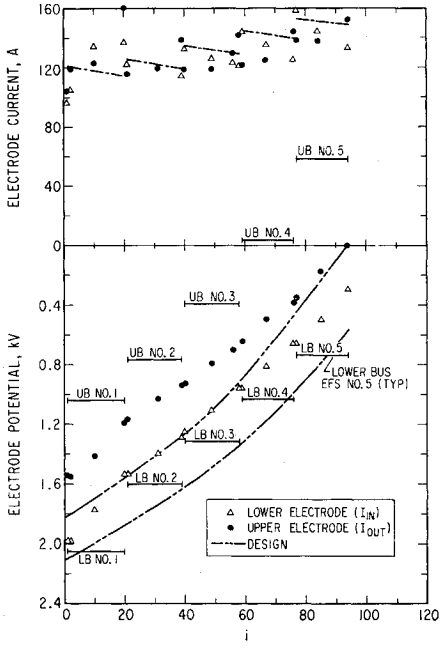

Fig. 7 Accelerator electrodynamic performance.

electrodes. With these voltages and current traces and the EFN resistance (r_i and ρ_i), a plot of the channel potential and current distribution can be obtained (Fig. 7). The current regulation capability of the EFS is demonstrated by the gross agreement between the design and the actual electrode currents. If each EFS is considered in detail, however, the downstream upper electrode tends to collect larger than average currents. This indicates that $J_x/J > 0$, except for EFS 1, where a low entrance σ results in an erratic current distribution (typically, $0.05 \leq J_x/J \leq 0.25$ for all downstream EFS's). The voltage distribution (Fig. 7) departs significantly from design in two respects: 1) a large $V_{l_1} - V_{x_1}$, which indicates a low σ at the channel entrance; and 2) a continued drop in $V_{l_i} - V_{u_i}$ as $i \to 94$, which is attributed to a lowering U potential due to two-dimensional effects. The decrease in potential difference with increasing electrode number is also accompanied by an increase in J_x/J where the direction of J_x is such that a smaller Hall potential is indicated, i.e., a smaller axial potential should be "built in" to the downstream EFS's. Such results have also been obtained in other accelerator experiments[4,5] and is unexplained at this writing.

When the flow arrives at the exit of the accelerator section of the channel, the induced potential U_e rises sharply from zero to a value $\propto B(t)$ after ~0.5 msec (Fig. 6d). It then increases when the accelerator current is turned on and decreases when the PFN shuts down. The dotted line superimposed on the trace shows the calculated output ($\propto B$) for the accelerator off U_{ef}. With $u_e \propto U_e/B_e$, the difference between the dotted line and the trace is then proportional to the velocity increase. This difference 1) increases as the number of powered electrodes increases and 2) increases toward the end of the test period. This is demonstrated in Fig. 8 where the ratio $(U_e/B_e)_n/(U_e/B_e)_f$ is shown relative to design values for the channel powered by 2, 3, or 5 EFS's. The initial velocity increase is reasonably close to the design value. The velocity continues to increase during the test period as a result of the hot-shot mass-flow decay and constant power input from the EFS.

Figure 6e shows the stagnation pressure at the accelerator exit. The trace is similar to U_e (except for the magnetic field dependence that is evident in U_e). The magnitude of the stagnation pressure just prior to accelerator operation p_{tf} agrees reasonably well with a one-dimensional expansion calculation [i.e., typically, $0.75 \leq p_{tf}/(\rho u^2)_{\text{cal}} \leq 1.1$]. Since $(\rho u)_n = (\rho u)_f$ at any accelerator axial location for steady flow, $p_{tn}/p_{tf} \approx u_{en}/u_{ef}$ and the remarks above relative to the time dependence of u_e also apply here. Figure 8 shows the results of the stagnation pressure measurements, which agree well with design values, and the results for u_{en}/u_{ef}, which were deduced from the U_e measurements.

Figures 6f and 6g show static pressure traces obtained at specific points along the accelerator length. The absolute value of the static pressure at each location prior to accelerator operation is somewhat higher than predicted by a one-dimensional calculation; i.e., typically, $1.2 \leq p/p_{\text{cal}} \leq 2$, which indicates flow nonuniformities. These static pressure measurements can be related to the change in the enthalpy since at constant γ, $p \propto \rho h \propto h/u$. Therefore,

$$p_n/p_f = (h_n/h_f)(u_{en}/u_{ef})^{-1}$$

and p_n/p_f should vary as the reciprocal of the stagnation pressure ratio p_{tn}/p_{tf}. This behavior is seen in Fig. 6f and 6e, where again dotted lines have been superimposed for the power-off condition. Figure 8 shows the results of such pressure measurements. Since the majority of points are somewhat higher than design, excess heating is present in the channel at accelerator turn-on [$(h_n/h_f)_{\text{are}} \approx 1.04$], which is consistent with the low σ in EFS 1. Increased heating at the end of the test period again results from decreasing mass flow at constant volumetric power input.

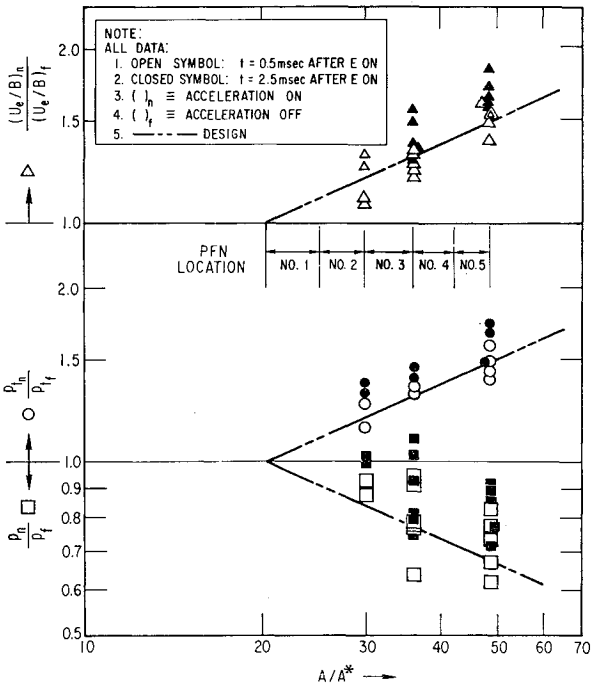

Fig. 8 Accelerator gasdynamic performance.

Some general comments on the physical condition of the accelerator after repeated operation are in order. Since the heat transferred to the walls during the test time is quite small, very little wall damage was observable. Typically, on the order of five runs were made before the channel was dismantled, and this was always done to replace a few electrodes that would protrude slightly ($\leq$0.01 in.) into the flow. No evidence of "breakdown" between adjacent or opposite electrodes was ever found from postrun checkout of the accelerator channel or could be inferred from measurements obtained during a run. In addition, there was no systematic change in any measured parameter that could be correlated with the number of runs on the channel.

VI. Concluding Remarks

The performance of a pulsed hypervelocity MHD wind tunnel has been investigated relative to a one-dimensional design. The tunnel consists of a hot-shot-type source, a capacitively powered magnetic field, and a segmented (94) electrode MHD channel powered by a unique electrode feed system (EFS). The hot shot produces a 9000°K, 1400-atm, potassium seeded nitrogen source gas that is expanded to 5.5 atm and 4000°K at the accelerator entrance where a crossed magnetic field of 4 wb/m^2 has been established. When steady flow is established in the accelerator, the EFS is switched on producing a constant current of approximately the design value. After a 3-msec quasi-steady test period, the EFS is switched off. This switch-on/switch-off capability of the EFS facilitates performance evaluation. Results obtained from instrumentation specially developed to cope with the time dependent electric and magnetic fields associated with the experiment indicate that:

1) On centerline, the velocity increases from u_e 16 kft/sec to $u_e \approx$ 24 kft/sec (as per design) ~0.5 msec after EFS switch-on.

2) On centerline, $h \approx$ const (as per design) 0.5 msec after EFS switch-on.

3) Centerline u_e increases further to 27 kft/sec and centerline h_e increases by ~20% prior to EFS switch-off, as a result of constant power input at decreasing mass flow.

4) The ratio of axial to accelerating current is $0.05 \leq J_x/J \leq 0.25$ (i.e., induced Hall potentials do not match those

impressed by the EFS). This is believed to result from nonuniformities in the flow and two-dimensional effects in the channel.

In general, the facility performs well relative to the one-dimensional design; however, problems associated with flow nonuniformities need to be solved since these effects have a significant influence upon the detailed behavior of the accelerator. In particular, the reason for a low U_e, the decreasing E with axial distance, and the slightly high, static pressures require investigation. In addition, the questions as to why σ is low at the channel entrance and why $J_x/J \neq 0$ need answering.

References

[1] Boison, J. C. and Ring, L. E., "A Low Density Hypervelocity for Developmental Testing," *Proceedings of the 8th Annual Air Force Systems Command Science and Engineering Symposium*, San Francisco, Calif., Oct. 1961.

[2] Leonard, R. L. and Rose, P. H., "Feasibility of a High Performance Aerodynamic Impulse Facility," *AIAA Journal*, Vol. 6, No. 3, March 1968, pp. 448–457.

[3] Templemeyer, K. E., Windmueller, A. K., and Rittenhouse, L. E., "Development of a Steady Flow J × B Accelerator for Wind Tunnel Application," TDR-64-261, Dec. 1964, Arnold Engineering Development Center, Tenn.

[4] Ring, L. E., "Status of MHD Accelerators for Test Facilities," TDR-65-229, Feb. 1966, Arnold Engineering Development Center, Tenn.

[5] Harris, C. J. et al., "A High Density Shock Tunnel Augmented by a Faraday MHD Accelerator," *Proceedings of the 4th Hypervelocity Techniques Symposium*, Arnold Engineering Development Center, Arnold AFS, Tenn., Nov. 1965, pp. 234–273.

[6] Mirels, H., "Analytical Solution for Constant Enthalpy MHD Accelerator," *AIAA Journal*, Vol. 2, No. 1, Jan. 1964, pp. 145–146.

[7] Van Der Bliek, J. A., "Further Development of Capacitance and Inductance Driven Hot Shot Tunnels," *Proceedings of the 2nd Hypervelocity Techniques Symposium*, Univ. of Denver, Denver, Colo., March 1962.

[8] Bird, K. D., Martin, J. F., and Bell, T. J., "Recent Developments in the Use of the Hypersonic Shock Tunnel as a Research and Development Facility," *Proceedings of the 3rd Hypervelocity Techniques Symposium*, Univ. of Denver, Denver, Colo., March 1964.

[9] Grabowsky, W. R., "Research and Experimentation, MHD Wind Tunnel Program Semiannual Technical Report," TDR-469(5240-10)-2, April 1965, The Aerospace Corp., El Segundo, Calif.

[10] Weber, R. E. and Templemeyer, K. E., "Calculation of the DC Electrical Conductivity of Equilibrium Nitrogen and Argon Plasma with and without Alkali Metal Seed," TDR-64-19, July 1964, Arnold Engineering Development Center, Tenn.

[11] Mirels, H., Gold, R. R., and Mullen, J. F., "Minimum Length MHD Accelerator with Constant Enthalpy," *AIAA Journal*, Vol. 3, No. 6, June 1965, pp. 1191–1192.

[12] Ring, L. E., "Optimization of MHD Crossed-Field Accelerators and Generators," *5th Symposium on Engineering Aspects of MHD*, Massachusetts Institute of Technology, Cambridge, Mass., April 1964.

[13] Bartz, D. R., "An Approximation Solution of Compressible Turbulent Boundary-Layer Development and Convective Heat Transfer in Convergent-Divergent Nozzles," *Transactions of the American Society of Mechanical Engineers*, Nov. 1955.

[14] Burke, A. F. and Bird, K. D., "The Use of Zonical and Contoured Expansion Nozzles in Hypervelocity Facilities," *Advances in Hypervelocity Techniques, Proceedings of the 2nd Symposium on Hypersonic Techniques*, Plenum Press, New York, 1962, pp. 373–424.

[15] Grabowsky, W. R., Durran, D. A., and Spencer, D. J., "Hot Shot Gas Source for Pulsed MHD Accelerator," *AIAA Journal*, Vol. 5, No. 10, Oct. 1967, pp. 1181–1817.

[16] Templemeyer, K. E., Rittenhouse, L. E., and Wilson, D. R., "Experiments on a Faraday-Type MHD Accelerator with Series Connected Electrodes," *AIAA Journal*, Vol. 3, No. 11, Nov. 1965, pp. 2160–2162.

[17] Durran, D. A. and Grabowsky, W. R., "Electrode Feed System for a Segmented Electrode MHD Accelerator," *AIAA Journal*, Vol. 5, No. 9, Sept. 1967, pp. 1714–1715.

[18] Grabowsky, W. R., Durran, D. A., and Spencer, D. J., "Development of a 9000°K 1400-atm Hot Shot Gas Source for Pulsed MHD Accelerator," TR-669(6240-10)-6, April 1966, The Aerospace Corp., El Segundo, Calif.

[19] Harris, C. J., Malin, J. R., and Rogers, D. A., "Measuring Techniques Applied in an MHD Augmented Shock Tunnel," *Institute of Electrical and Electronics Engineers Transactions Aerospace and Electronic Systems, AES-3*, No. 3, May 1967.

[20] Grabowsky, W. R. and Durran, D. A., "A Gauge for Measuring Impulsive Pressure in a Container Subjected to Large Time Varying Applied Voltages," RSI, 39, 35–38, Jan. 1968, The Aerospace Corp., El Segundo, Calif.

[21] Grabowsky, W. R., Durran, D. A., and Rognlien, T., "Pressure Gauge for High Electrical Noise Level Environment," TR-0158(3240-10)-9, March 1968, The Aerospace Corp., El Segundo, Calif.

[22] Grabowsky, W. R., Durran, D. A., and Gerard, M. E., "A Pressure Gauge for Plasmas Subjected to Large Dynamic Electric and Magnetic Field," *Review of Scientific Instruments*, Vol. 38, Aug. 1967, pp. 1160–1161.

[23] Boison, C. J. and Curtiss, H. A., "An Experimental Investigation of Blunt Body Stagnation Point Velocity Gradient," *ARS Journal*, Vol. 29, Feb. 1959, pp. 130–135.